

# Variable circumstellar activity of V351 Orionis

R. Choudhury, H. C. Bhatt, and G. Pandey

Indian Institute of Astrophysics, Bangalore 560034, India  
e-mail: rumpa@iiap.res.in

Received 8 August 2010 / Accepted 2 November 2010

## ABSTRACT

**Context.** Emission and absorption line profiles which are formed in the interaction of pre-main sequence stars and their circumstellar environment are found to be variable at various timescales.

**Aims.** We investigate the patterns and timescales of temporal line profile variability in order to explore the dynamical circumstellar environment of the pre-main sequence Herbig Ae star V351 Ori.

**Methods.** We obtained 45 high-resolution ( $R \sim 28\,000$ ) spectra of V351 Ori at timescales of hours, days, and months. We analysed the  $H\alpha$  line profiles and also examined the  $H\beta$ , NaD1 and NaD2 line profiles to explore the nature of the spectroscopic variability.

**Results.** The  $H\alpha$  line profiles showed strong variations over all timescales. The shape of the profiles changed over timescales of a day. Single as well as simultaneous event(s) of blue-shifted and red-shifted transient absorption components, i.e. signatures of outflow and infall, were also observed in the  $H\alpha$  line profiles. The shortest period of variation in the transient absorption components was  $\leq 1$  hour. All transient absorption events were found to decelerate with a rate of a few to fractions of  $\text{m s}^{-2}$ . The depth and width of the transient absorption components were also changing with time. The presence of elongated red-shifted components at some epochs supports the episodic nature of accretion.

**Conclusions.** Variable emission and absorption components detected in  $H\alpha$  line profiles show the dynamic nature of interaction between V351 Ori and its circumstellar environment. The  $H\alpha$  non-photospheric profiles of the star most probably originate in the disk wind. Episodic accretion of gaseous material at a slow rate and outflow of clumpy gaseous material are still occurring in V351 Ori at an age of  $\sim 6.5$  Myr. Dynamic magnetospheric accretion and disk wind emerge as the most satisfactory model for interpreting the observed line profile variations of V351 Ori.

**Key words.** stars: pre-main sequence – circumstellar matter – stars: individual: V351 Ori – techniques: spectroscopic – line: profiles

## 1. Introduction

Herbig Ae/Be stars are revealed pre-main sequence (PMS) emission line stars with masses of  $\sim 1.5$  to  $10 M_{\odot}$  and typical ages of  $\sim 10^6$  years with spectral types earlier than  $F0$ . Balmer emission lines of hydrogen and infrared (IR) excess emission produced by thermal emission of circumstellar dust grains are the prominent characteristics of Herbig Ae/Be stars. Both of these signatures originate in the circumstellar material around these stars and the interaction between them. It has been well established that circumstellar material, i.e. dust and gas around the Herbig Ae/Be stars, are distributed in disks (e.g. Maheswar et al. 2002, and references therein). Significant variations in shape and intensity of permitted and forbidden emission line profiles, originating in the accretion or outflow events of the interaction between the central star and its surrounding material, are observed in many Herbig Ae/Be stars (Hamann & Persson 1992; Hamann 1994; Reipurth et al. 1996). Optical spectroscopic studies of emission line profiles of a few Herbig Ae/Be stars are reported in the literature in e.g. Grinin et al. (1994); de Winter et al. (1999); Grinin et al. (2001); Natta et al. (2000); Mora et al. (2002, 2004); Guimarães et al. (2006). Natta et al. (2000) reported the evidence for episodic rather than continuous accretion in Herbig Ae star UX Ori. Mora et al. (2002, 2004) reported transient absorption components (TACs) in several Balmer and metallic lines of a few Herbig Ae type stars, which are supposed to be created by moving gaseous blobs around these stars. These studies discussed the dynamical circumstellar environment around Herbig Ae/Be stars which show strong  $H\alpha$  emission.

Manoj et al. (2006) showed that the emission line activity of Herbig Ae/Be stars substantially decreases by  $\sim 3$  Myr, which agrees well with the inner disk survival timescale i.e.  $\sim 3$  Myr as suggested by Hernández et al. (2005, 2009) for the early spectral type stars such as B, A, and F types. The dissipation of optically thick disks beyond  $\sim 3$  Myr to the onset of young main sequence stars with a debris disk can be caused by various disk dispersal processes such as photoevaporation, planet formation, etc. Herbig Ae/Be stars with weak emission lines and moderate IR excess can be considered as the precursor of the young main sequence stars with IR excess and no gaseous emission lines, e.g.  $\beta$  Pic and Vega. Understanding the nature of accretion and circumstellar material of comparatively less active Herbig Ae/Be stars of age  $\geq 3$  Myr are important because these processes eventually set the stage for planet formation. However, detailed studies of weak emission line Herbig Ae/Be stars that cover hours, days, and months are not available in the literature.

V351 Orionis (V351 Ori, HIP 27059, HD 38238) is a weak  $H\alpha$  emission line Herbig Ae star that showed photometric and spectroscopic variabilities over various timescales (e.g. van den Ancker et al. 1996; Balona et al. 2002, and references therein). The classification of V351 Ori as a Herbig Ae star has been confirmed by several authors, e.g. van den Ancker et al. (1996); Vieira et al. (2003); Hernández et al. (2005). Grady et al. (1996) analysed the ultraviolet (UV) spectra of V351 Ori and did not find any absorption component, i.e. signatures of stellar wind or accretion, in the spectra. van den Ancker et al. (1996) presented photometric and spectroscopic observations of V351 Ori

and found that it transformed into an almost non-variable star from a strong photometric variable within a short period of  $\sim 14$  years. [van den Ancker et al.](#) reported that the  $H\alpha$  profile of V351 Ori was of an inverse P Cygni type and also showed a high infrared excess emission. Inverse P Cygni profiles are signatures of the accretion of circumstellar material onto the central object and are characterised by blue-shifted emission with red-shifted absorptions or systematically enhanced red shifted absorptions. V351 Ori shows  $\delta$  Scuti type pulsation ([Marconi et al. 2000](#)), which is another characteristic of pre-main sequence stars of mass  $\geq 1.5 M_{\odot}$  as they cross the pulsation instability towards their contraction to the main sequence. [Balona et al. \(2002\)](#) obtained simultaneous multi-colour photometric and spectroscopic observations of V351 Ori to investigate the nature of the pulsation of V351 Ori. [Balona et al.](#) also reported a variable inverse P Cygni type  $H\alpha$  profile with a variation on a timescale of a day with complete absence of emission at some epochs. [Vieira et al. \(2003\)](#) observed an inverse P Cygni type  $H\alpha$  emission line profile in V351 Ori and also suggested that V351 Ori might be an evolved Herbig Ae star, because it shows weak emission lines. [Hernández et al. \(2005\)](#) also reported a low equivalent width of  $H\alpha$  i.e.  $EW_{\lambda}[H\alpha] = -0.9 \text{ \AA}$  and associated V351 Ori with Ori OB1bc region. These signatures hint at an active interaction of the weak  $H\alpha$  emission line young star V351 Ori with its circumstellar environment.

In this work we present high-resolution spectroscopic observations of V351 Ori along with optical *BVRI* observations. We discuss the dynamic circumstellar gaseous environment of the star in the light of available models of star-disk interaction. Observations and data reduction are discussed in Sect. 2. In Sect. 3 we present the details of the spectra and the analysis of the transient absorption components detected in the spectra. A discussion of the kinematics of the observed transient absorption components, an estimate of the disk mass and a qualitative interpretation of the  $H\alpha$  line profile variation are presented in Sect. 4. We present our conclusion in Sect. 5.

## 2. Observations and data reduction

Fortyfive high-resolution spectra of V351 Ori were obtained during October 2008 to April 2009 with a fibre-fed cross-dispersed echelle spectrometer ([Rao et al. 2005](#)) at the 2.3 m Vainu Bappu Telescope of Vainu Bappu Observatory (VBO), Kavalur, India<sup>1</sup>. The log of the observations is given in Table 1. The resolving power of the spectrometer set-up used for observation is  $\sim 28\,000$  and the attached  $2K \times 4K$  CCD gives a dispersion of  $\sim 0.025 \text{ \AA}$  per pixel. The typical integration time of each spectrum was 45 min. Bias subtraction, flat field correction and scatter light removal were carried out for all the spectra with the standard tasks available in the Image Reduction and Analysis Facility (IRAF)<sup>2</sup>. The Th-Ar lamp was used for wavelength calibration. The final spectra that were used for our analysis cover the wavelength region from  $\lambda 4250 \text{ \AA}$  to  $\lambda 7900 \text{ \AA}$ . The CCD used for observation did not cover the full echelogram, and as a consequence there are some gaps in the wavelength coverage of the observed spectra. However, we optimised the CCD position accordingly to cover the wavelength regions of  $H\alpha$ ,  $H\beta$ , NaD1, NaD2 and several other photospheric lines. Atmospheric lines were also used

<sup>1</sup> [http://www.iiap.res.in/vbo\\_vbt](http://www.iiap.res.in/vbo_vbt)

<sup>2</sup> The IRAF software is distributed by the National Optical Astronomy Observatory under contact with National Science Foundation <http://iraf.noao.edu/>.

**Table 1.** Observation log of the echelle spectroscopy of V351 Ori.

Date	HJD – 2 454 000	$t_{\text{exp}}$ (s)	$H\alpha$ profile type <sup>a</sup>
2008-10-27	767.28–767.41	$2700 \times 4$	IV-R, inverse P Cygni
2008-10-30	770.38	$2700 \times 1$	II-R, double peak
2008-12-11	812.32	$2700 \times 1$	IV-R
2008-12-28	829.10–829.32	$2700 \times 6$	IV-R
2008-12-29	830.10–830.37	$2700 \times 8$	IV-R
2009-01-17	849.11–849.22	$2700 \times 4$	III-R, double peak
2009-01-18	850.10–850.32	$2700 \times 4$	III-R
2009-01-19	851.09–851.35	$2700 \times 5$	III-R
2009-01-20	852.07–852.18	$2700 \times 2$	III-R
2009-03-02	893.11–893.15	$2700 \times 2$	III-R
2009-03-03	894.20	$2700 \times 1$	II-R
2009-03-29	920.16	$2700 \times 1$	IV-R
2009-03-30	921.07–921.11	$2700 \times 2$	II-R
2009-03-31	922.08	$2700 \times 1$	III-R
2009-04-26	948.07	$2700 \times 1$	III-R
2009-04-27	949.07	$2700 \times 1$	II-R
2009-04-28	950.07	$2700 \times 1$	II-R

**Notes.** <sup>(a)</sup> Based on the classification scheme adopted from [Reipurth et al. \(1996\)](#). Type II-R profile represents a double peak profile where the red-sided peak exceeds the strength of the blue-sided peak by half. Type III-R also represents double peak profile with the red-sided peak less than half the strength of the blue-sided peak. Type IV-R represents the inverse P Cygni profile.

to check the wavelength calibration. These wavelength calibrations of the final spectra are accurate up to  $\pm 0.01 \text{ \AA}$ .

V351 Ori was observed on 11 November 2009 with the Bessell broad band filters *B* ( $5 \times 5$  s), *V* ( $4 \times 2$  s), *R* ( $4 \times 1$  s) and *I* ( $5 \times 1$  s) of the Himalayan Faint Object Spectrograph Camera (HFOSC) mounted on the 2 m Himalayan Chandra Telescope (HCT) of the Indian Astronomical Observatory (IAO), Hanle, India<sup>3</sup>. Data were reduced with the standard tasks in IRAF.

## 3. Results and analysis

### 3.1. Description of echelle spectra

Herbig Ae/Be stars show both short and long term variabilities in their spectra. To explore the short to long term variations of the line profiles we obtained high-resolution spectra on timescales as short as an hour to the longest coverage of  $\sim 7$  months. All 45 spectra cover the wavelength regions of  $H\alpha$ ,  $H\beta$ , NaD1, NaD2 and several other photospheric lines. Typical signal- to-noise ratios ( $S/N$ ) are  $< 10$  to  $12$  at  $H\beta$ ,  $15$  to  $30$  at NaD1 and NaD2 and  $\geq 30$  to  $60$  at  $H\alpha$ . We note that [O I]  $\lambda 6300 \text{ \AA}$  emission line was present in several spectra. [Balona et al. \(2002\)](#) also reported the detection of a narrow emission line of [O I]  $\lambda 6300 \text{ \AA}$  at a velocity of  $+7.5 \text{ km s}^{-1}$ . However, the line centre of [O I]  $\lambda 6300 \text{ \AA}$  in our observed spectra remained constant at laboratory wavelength, as did the other telluric lines throughout our observing runs. We therefore conclude that the [O I]  $\lambda 6300 \text{ \AA}$  emission line in our observed spectra is of telluric origin. We did not find any detectable emission in the  $H\beta$ , NaD1 and NaD2 line profiles, including the other photospheric lines typical to an A7 type stars within the noise level of our observed spectra. Though the  $H\alpha$  line profiles were dominated by variable absorption components, but nominal to significant variable emission components were also observed. Below we describe in detail the behaviour of different line profiles. To compare the spectra obtained in

<sup>3</sup> <http://www.iiap.res.in/centers/iao>

different epochs one needs to normalise the spectra in a similar fashion. The normalisation of the echelle spectra by fitting the continuum is tricky, because each order displays a limited wavelength coverage (in this case  $\sim 40$  Å). However, with the synthetic spectra of the star as the guiding standard, a better fit to the continuum and accordingly a common normalisation of all spectra can be obtained. As we shall discuss below, synthetic spectra are also essential to identify the circumstellar component in the line profiles that are dominated by absorption components.

### 3.2. Stellar parameters and synthetic spectra

Balona et al. (2002) estimated the effective temperature ( $T_{\text{eff}}$ ), rotational velocity ( $v \sin i$ ), and  $\log g$  (logarithm of the surface gravity) of V351 Ori in order to generate the synthetic spectra of the star. Ripepi et al. (2003) estimated effective temperature ( $T_{\text{eff}} \sim 7425\text{--}7600$  K) of the star using the pulsation models. The average effective temperature of Ripepi et al. matches quite well with the estimated value of 7500 K by Balona et al. Recent studies on the stellar parameters of Herbig Ae/Be stars showed that the typical value of  $\log g$  is  $\sim 4.0$ , which also gives a reasonable fit to the photospheric wings of the  $H\alpha$  and  $H\beta$  profiles of emission line Herbig Ae/Be stars. We used the model atmosphere from the Kurucz model atmosphere database<sup>4</sup> for an A7 III star with  $T_{\text{eff}} = 7500$  K as adopted from Balona et al. (2002) and  $\log g = 4.00$ . We used  $v \sin i = 102$  km s<sup>-1</sup> (Balona et al. 2002) and a micro turbulent velocity of 2 km s<sup>-1</sup> as suggested by Dunkin et al. (1997). Detailed synthetic spectra were computed with the interactive data language (IDL) interface SYNPLIT (Hubeny, priv. comm.) to the spectrum synthesis programme SYNSPEC Hubeny & Lanz (2000), utilising the adopted Kurucz model atmosphere. The linelist provided in SYNSPEC is used to generate the synthetic spectra.

We convolved the synthetic spectra with the rotational profile of V351 Ori and the instrumental profile of the echelle spectrometer with SYNPLIT and ROTINS<sup>5</sup>. In Figs. 1 and 2 we display some of the representative photospheric line profiles and overplot the convolved synthetic spectra. Because the observed photospheric and synthetic line profiles show a good match over long wavelength ranges, we did not attempt to fit the photospheric lines rigorously to obtain the stellar parameters. We used the convolved synthetic spectra to identify unblended photospheric lines to obtain the radial velocity of the the star. We used Fe I, Fe II, and Ca I lines in a wavelength range from  $\lambda 5000$  to  $\lambda 6500$  Å (such as Fe II  $\lambda 4923.827$  Å, Fe I  $\lambda 5001.862$  Å, Fe I  $\lambda 5429.696$  Å, Fe II  $\lambda 5534.847$  Å, Fe I  $\lambda 5615.644$  Å, Ca I  $\lambda 6102.723$  Å, Ca I  $\lambda 6122.217$  Å, Ca I  $\lambda 6439.075$  Å) to measure the radial velocity of the star. We estimate the average heliocentric radial velocity of the star as  $+11_{-3}^{+4}$  km s<sup>-1</sup>, which is similar to the estimated radial velocity i.e.  $+13$  km s<sup>-1</sup> by Balona et al. (2002). We synthesised the photospheric  $H\alpha$  line profile following the same procedures.

### 3.3. $H\alpha$ line profiles

We display all the  $H\alpha$  emission line profiles in the rest frame velocity of V351 Ori and overplot the photospheric components in Figs. 3a to 6a. We also mark the spectra by their date of observation and the modified heliocentric Julian day (MHJD)

<sup>4</sup> <http://kurucz.harvard.edu/>

<sup>5</sup> <http://nova.astro.umd.edu/Synspec43/synspec-frames-rotin.html>

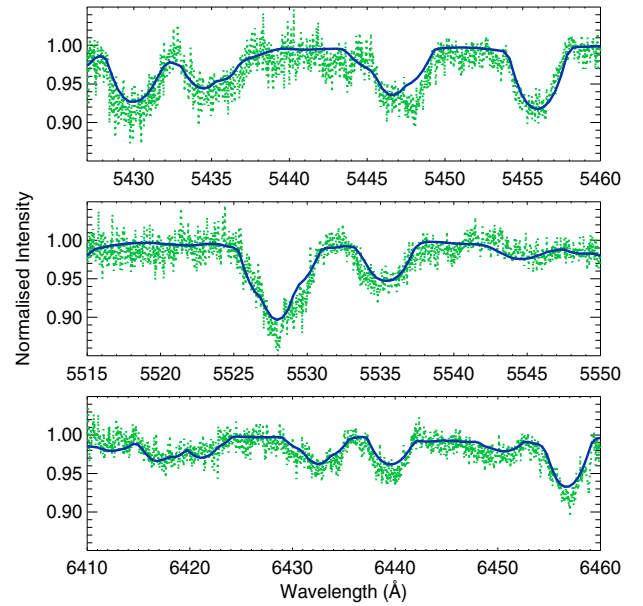


**Fig. 1.** Average photospheric line profiles of V351 Ori on 29 December 2009 (dotted green line). Synthetic spectra in the same wavelength range are overplotted (solid blue line). The prominent photospheric lines are Fe I 5429.696, 5434.523, 5445.042, 5446.871, 5446.916, 5455.441 and 5455.609 in the first row, Sc II 5526.790, Mg I 5528.405 and Fe II 5534.847 in the second row, and Fe I 6430.844, Fe II 6432.680, Ca I 6439.075, and Fe II 6456.383 in the third row. (This figure is available in colour in electronic form.)

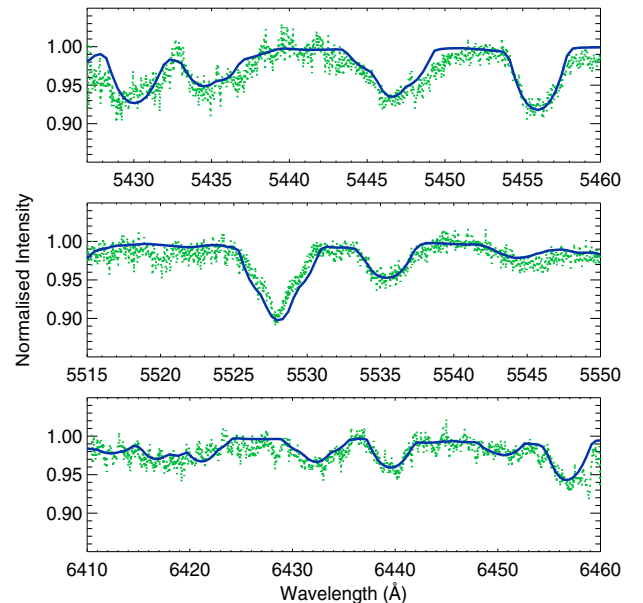


**Fig. 2.** Average photospheric line profiles of V351 Ori of 17 to 19 January 2009 (dotted green line). Synthetic spectra in the same wavelength range are overplotted (solid blue line). (This figure is available in colour in electronic form.)

defined by heliocentric Julian day (HJD)–2 454 000. We subtract the photospheric component from the observed spectrum

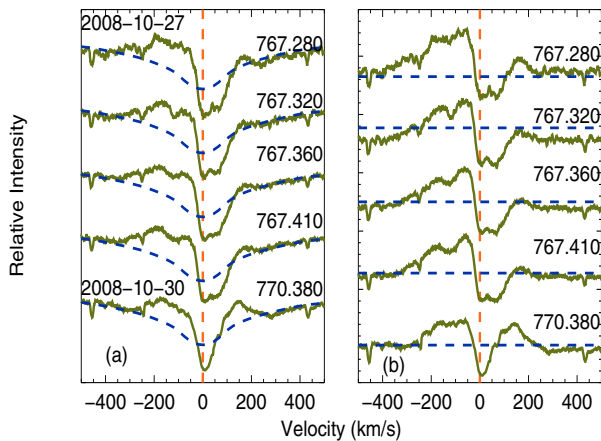


**Fig. 3. a)**  $H\alpha$  line profiles (green solid lines) of V351 Ori of a couple of days in October 2008. The synthetic  $H\alpha$  line profiles (blue dashed lines) are overplotted on each spectrum. Modified Julian days are displayed against the respective spectrum. The vertical red dashed line represents the rest frame velocity of the star. **b)** Residual spectra of  $H\alpha$  line profiles in the same epochs. Horizontal blue dashed lines represent the zero absorption levels. (This figure is available in colour in electronic form.)

and show the residual spectrum in Figs. 3b to 6b. The zero level in the residual spectrum is described as the zero absorption level. As discussed before, profile variations on a timescale of days to months are quite common to V351 Ori. We also observed both blue- and red-shifted absorption components of various widths and depths in several epochs. These features are also seen in other Herbig Ae/Be stars such as UX Ori, BF Ori, SV Cep, WW Vul, and XY Per, see e.g. Mora et al. (2002, 2004) and references therein. These features are called transient absorption components (TACs) because they are sporadic in nature and last for a few days only. Transient absorption components can be divided into two categories, i.e. blue-shifted absorption components (BACs) and red shifted absorption components (RACs). The chemical compositions and kinematics of the transient absorption components have been discussed by several authors, e.g. Natta et al. (2000); Mora et al. (2002, 2004). We discuss the profile variations in detail in the subsequent sections. We quote the velocity of the broad wings from the residual spectra and that of the transient absorption components from the observed normalised spectra.

### 3.4. Line profile variations

Previous studies of e.g. van den Ancker et al. (1996), Balona et al. (2002), and Vieira et al. (2003) reported that the average  $H\alpha$  emission line profiles of V351 Ori were inverse P Cygni types. From Table 1 it is evident that V351 Ori showed various profile shapes such as II-R and III-R, including inverse P Cygni types during our observation. Nightly variations of profiles from an average behaviour at a timescale of a day were also observed in several epochs. The type II-R profile of 2 March 2009 evolved into a type III-R on 3 March 2009. Another incident of a rapid variation in profile shapes was observed during 29 to 31 March 2009. Three different types of  $H\alpha$  profiles, namely IV-R, II-R, and III-R, were observed on these consecutive nights. The flip-over from type II to type III profiles, i.e. the change in strength of blue- and red-shifted emission

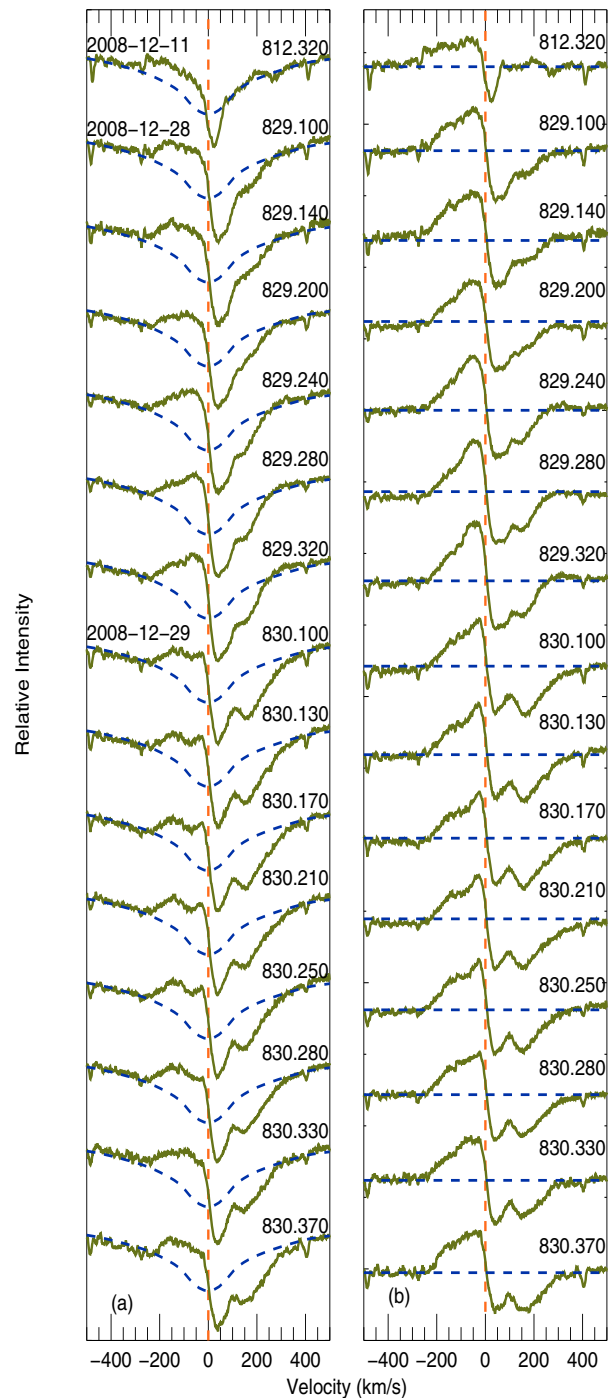


**Fig. 4. a)**  $H\alpha$  line profiles (green solid lines) of V351 Ori of a few days in December 2008. Synthetic  $H\alpha$  line profiles (blue dashed lines) are overplotted on each spectrum. Modified Julian days are displayed against the respective spectrum. The vertical red dashed line represents the rest frame velocity of the star. **b)** Residual spectra of  $H\alpha$  line profiles in the same epochs. Horizontal blue dashed lines represent the zero absorption levels. (This figure is available in colour in electronic form.)

peaks in a double-peak profile, was also reported by Vieira et al. (2003) in PDS 018 and PDS 024, but on longer timescales that were separated by months to year respectively. We also observed

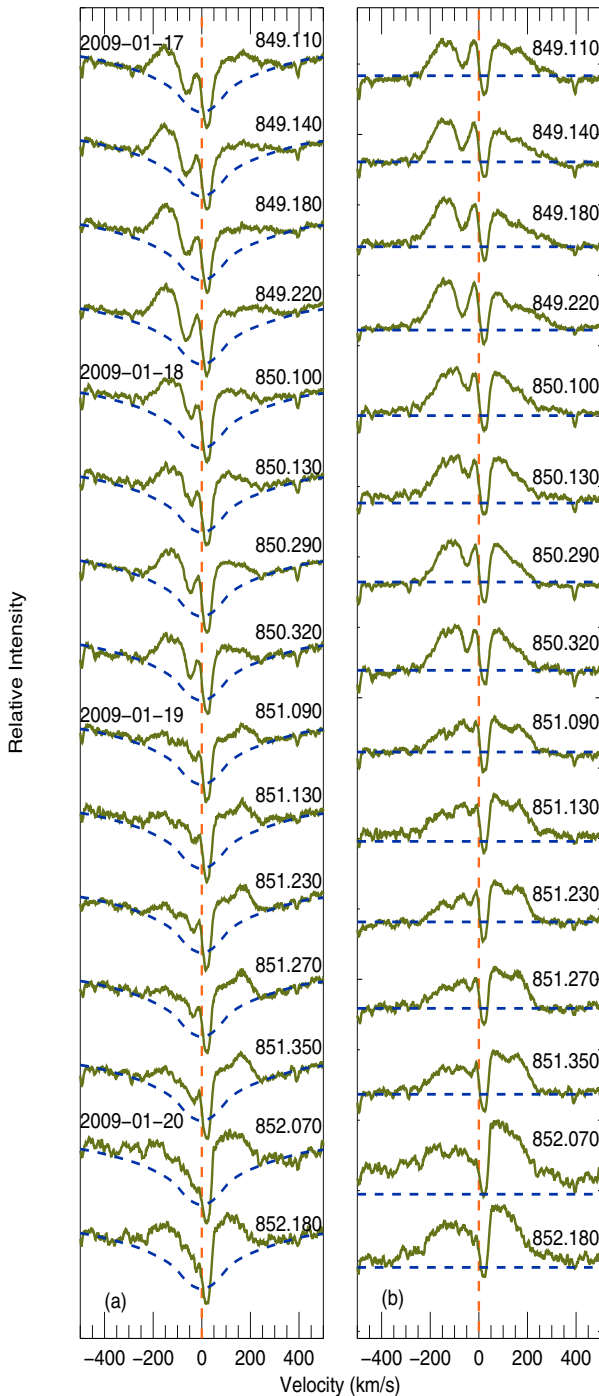


**Fig. 5.** **a)**  $H\alpha$  line profiles (green solid lines) of V351 Ori of a few days in January 2009. Synthetic  $H\alpha$  line profiles (blue dashed lines) are overplotted on each spectrum. Modified Julian days are displayed against the respective spectrum. The vertical red dashed line represents the rest frame velocity of the star. **b)** Residual spectra of  $H\alpha$  line profiles in the same epochs. Horizontal blue dashed lines represent the zero absorption levels. (This figure is available in colour in electronic form.)

two prominent incidents of infall and outflow in the  $H\alpha$  profiles on 28 to 29 December, 2008 and 17 to 20 January, 2008 respectively. The infall event was seen in the  $H\beta$  profiles as well

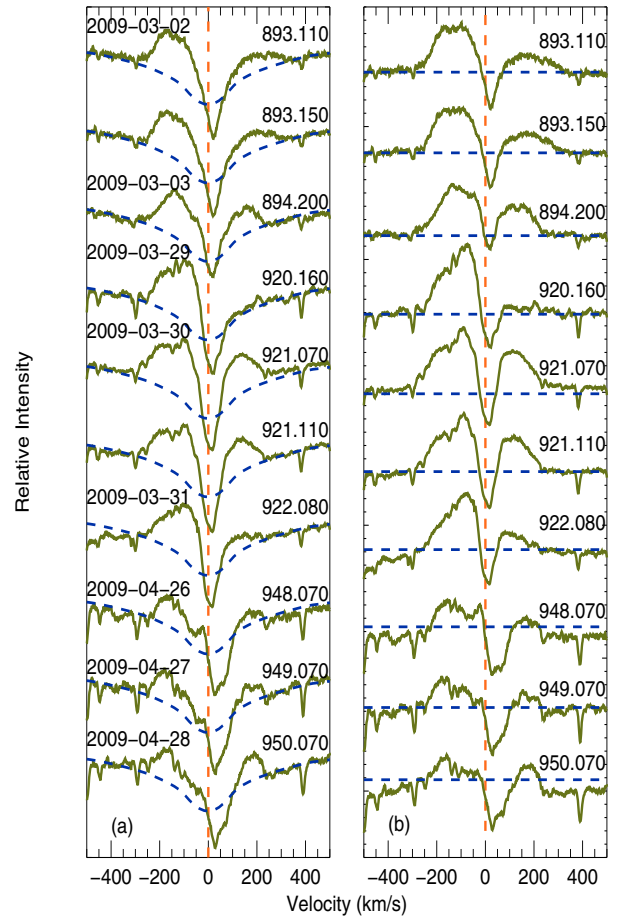


**Fig. 6.** **a)**  $H\alpha$  line profiles (green solid lines) of V351 Ori of some days in March and April 2009. Synthetic  $H\alpha$  line profiles (blue dashed lines) are overplotted on each spectrum. Modified Julian days are displayed against the respective spectrum. The vertical red dashed line represents the rest frame velocity of the star. **b)** Residual spectra of  $H\alpha$  line profiles in the same epochs. Horizontal blue dashed lines represent the zero absorption levels. (This figure is available in colour in electronic form.)

(Fig. 11). We also checked a few photospheric metallic lines in these epochs that were separated by nearly two weeks (Figs. 1 and 2) and did not find any variation in those profiles, which also indicates that there was no significant variation in the stellar photosphere during the infall and outflow events.

We calculated the mean and temporal variance profile of  $H\alpha$  line profiles to investigate the characteristics of the variations. We calculated the mean profile by taking the average normalised intensity in each velocity interval of a given profile over all observed profiles. We show the average normalised  $H\alpha$  line profile of V351 Ori in Fig. 7. As suggested by Johns & Barri (1995), we define the temporal variance profile at each velocity interval as

$$\sum_v = \frac{\sum_{i=1}^n (I_{v,i} - \bar{I}_v)^2}{n - 1},$$

where  $n$  is the number of spectra,  $I_{v,i}$  is normalised intensity at a given velocity ( $v$ ) in each spectrum ( $i$ ), and  $\bar{I}_v$  is mean normalised intensity at a given velocity ( $v$ ) over all observed spectra. The normalised variance profile (shown as shaded area in

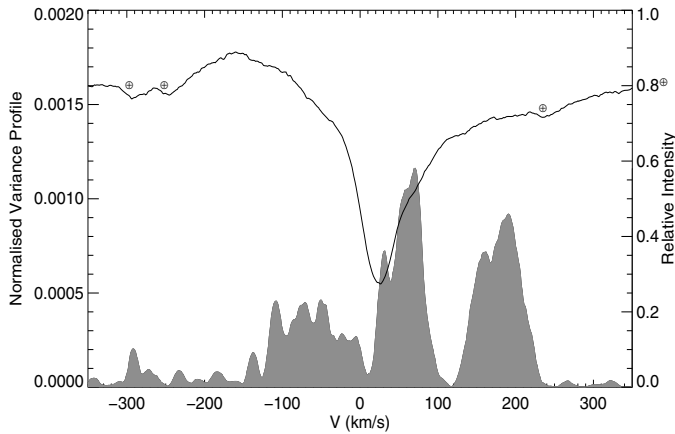


**Fig. 7.** Average  $H\alpha$  line profile (solid line) and variance profile (grey shaded area) of V351 Ori obtained using all spectra.

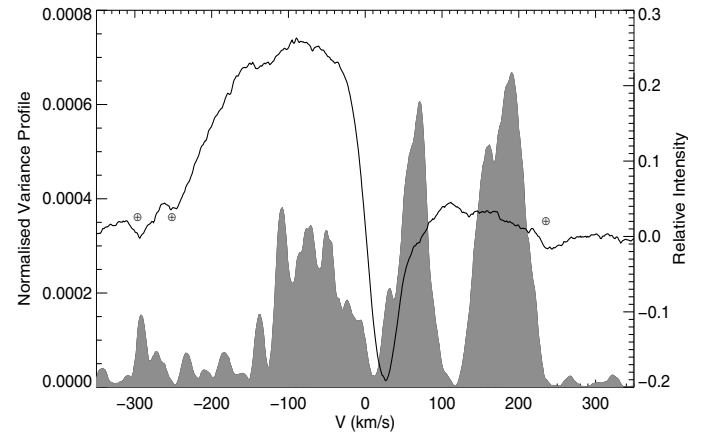


**Fig. 8.** Average  $H\alpha$  line profile (solid line) and variance profile (grey shaded area) of V351 Ori obtained using all residual spectra.

Fig. 7) can be obtained by dividing the temporal variance profile by the average profile. The normalised variance profile indicates that the behaviour of an individual spectrum observed at different epochs deviates substantially from the average profile. Most of the variability in  $H\alpha$  profile is on red side with two clearly distinguished features. There are significant variations on blue side as well, but the profile shows a single peak. A couple of outflow events were observed at different epochs separated by days to months, but they seem to have an approximate average velocity of  $-100 \text{ km s}^{-1}$ . We also observed simultaneous infall and outflow events of different durations at different velocities. It is obvious from Fig. 7 that the infall events occurred at two distinctly different velocities of e.g.  $\sim 60 \text{ km s}^{-1}$  and  $\sim 150 \text{ km s}^{-1}$ . In emission line stars, circumstellar emission first fills the photospheric absorption components and the residual flux emerges as *emission* from the star. If there is strong emission, the reduction of emission flux to cover up the photospheric absorption is not significant. However, for weak emission, where the  $H\alpha$  line profile is dominated by absorption rather than emission, a subtraction of photospheric component is necessary to achieve the true contribution caused by emission. Red-shifted narrow absorption components in Figs. 3a to 6a, which indicate infall of matter, are prominently visible beyond the photospheric profiles. Accordingly the subtraction of photospheric profiles are not crucial for comparative studies of these features. However, the broad blue- and red-shifted emission/absorption components at the wings sometimes appeared at the same level as the photospheric profiles. To make sure that we were not looking at the photospheric, but at the circumstellar components, we subtracted the photospheric spectra from the observed normalised spectra and plotted the profiles in Figs. 3b to 6b. The residual profiles also provide a better estimate of maximum velocity reached at the wings of the profiles, which are not contaminated by photospheric components. We define the maximum velocity of the profile at wings as the full-width-at-zero intensity of the residual spectra. We also calculate the average and variance profiles using residual spectra. The average profile in Fig. 8 is a double-peak profile with a strong blue to red asymmetry, i.e. III-R type, which is different from its counterpart in Fig. 7. The red-shifted absorption near the centre is similar to that of Fig. 7 and there is no change in the variance profiles in Figs. 7 and 8. In Fig. 8, the two peaks of the red-shifted variance profiles do not coincide with red-shifted emission peak of average profile of the residual spectra, which supports the presence of emission in most

epochs. Double peak profiles are supposed to form in stellar or disk winds contrary to inverse P Cygni profiles, which originate in the infall of materials. We shall discuss below the effects of accretion, winds, etc. on the profile shapes. Significant changes in the average profiles in Figs. 7 and 8 show that photospheric profile subtraction is necessary at least for weak  $H\alpha$  emission line stars.

### 3.5. Profile variations on 27 and 30 October, 2008

We observed a double-peak profile, e.g. a type III-R profile, on 27 October 2008 with moderate blue-shifted and weak red-shifted emission components just above the photospheric spectra (Fig. 3a). The blue-shifted emission component did not change much, but the red-shifted component gained strength and became comparable to its blue-shifted counterpart, i.e. there were nearly symmetric broad emission components on both sides of the central minima, and thus the profile shape evolved into a type II-R on 30 October. The maximum average velocity of the profile was  $\sim -350 \text{ km s}^{-1}$  and  $\sim 250 \text{ km s}^{-1}$  on 27 October, and  $\sim -300 \text{ km s}^{-1}$  and  $\sim 280 \text{ km s}^{-1}$  on 30 October at the blue and red wings respectively. We observed simultaneous inflow and outflow events on 27 October. The central broad asymmetric absorption feature ( $\sim 40 \text{ km s}^{-1}$ ) on 27 October was extended more towards the red region. It consisted of two barely resolved components with centres at  $\sim 6 \text{ km s}^{-1}$  and  $\sim 50 \text{ km s}^{-1}$ . This broad absorption might be a combination of two absorptions of nearly similar depths because of both the disk and the infall of the circumstellar material. The width of the central absorption was reduced on 30 October and seemed to represent a single absorption component at  $\sim 9 \text{ km s}^{-1}$ , which was nearly symmetric with the rest frame velocity of the star. We also observed a blue-shifted absorption component on 27 October superposed on the blue-shifted emission component, which is considered as a signature of the outflow. The full width at half maxima (FWHM) of the outflow increased with time, but its depth decreased (Table 2).

### 3.6. Profile variations on 11, 28 and 29 December, 2008

The  $H\alpha$  line profile on 11 December 2008 was of an inverse P Cygni type with a narrow absorption centred at  $\sim 30 \text{ km s}^{-1}$  (Fig. 4). It was one of the few profiles where the red component almost matched the photospheric component. During

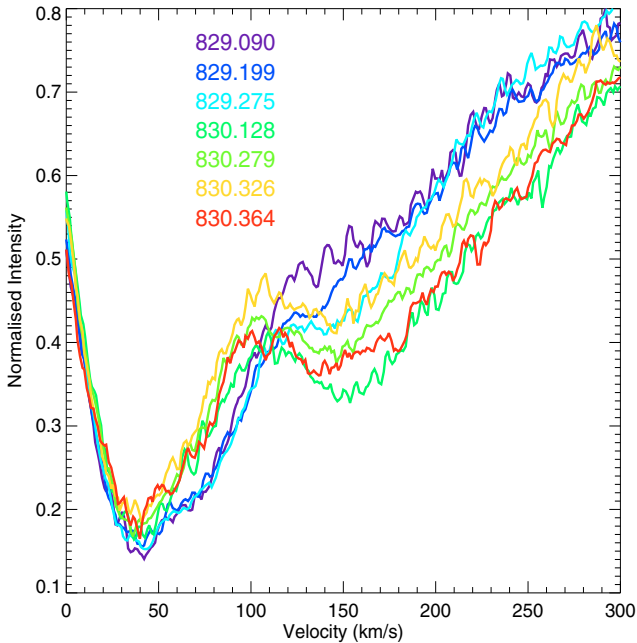


**Fig. 9.** Selected  $H\alpha$  emission line profiles on 28 and 29 December 2008 in the rest frame velocity of V351 Ori are overplotted. MHJD of the respective profiles are displayed using the same colours as of the profiles.

28 December and 29 December 2008 the  $H\alpha$  line profiles were also of the inverse P Cygni type. We observed the emergence of an infall event on 28 December and followed its evolution for several hours and until the next night. The depth of the RAC was less than the depth of the central absorption component, which became red-shifted and wider compared to its counterpart on 11 December. The nightly variations of the maximum velocity of the blue wings were between  $-250$  to  $-300$   $\text{km s}^{-1}$ , and that of the red absorption wings was  $300$   $\text{km s}^{-1}$  and it did not vary much throughout the night. On 29 December 2008 we observed both prominent infall and weak outflow events simultaneously (Fig. 4a MHJD 830.100 to 830.280). The RAC that emerged on 28 December became deeper and its centre was separated from the central absorption component, as a result of which the width of the central absorption component reduced (Fig. 9). The maximum velocity at the blue wings did not change, but the average maximum velocity at the red wings shifted to  $\sim 380$   $\text{km s}^{-1}$  on 29 December. The depth of the RAC varied throughout the observations on 28 and 29 December. We show the emergence and evolution of the RAC in Fig. 9. The velocity of the RAC was decelerated within a few hours from its starting point and then became constant at MHJD 830.21, where it remained until the end of the observation on 29 December (Table 2). All observed line profiles of 28 and 29 December showed a blue-shifted emission component whose strength increased after MHJD 829.1. We detected the outflow on top of the blue-shifted emission at MJHD 830.100 and could identify it clearly before MHJD 830.330. It gradually moved towards the central absorption features so the probable reason for its non-detection after MHJD 830.330 might be because the BAC came in the same line of sight of the central absorption.

### 3.7. Profile variations on 17 to 20 January, 2009

The  $H\alpha$  emission line profiles observed during 17 to 20 January 2009 are mostly dominated by both blue- and

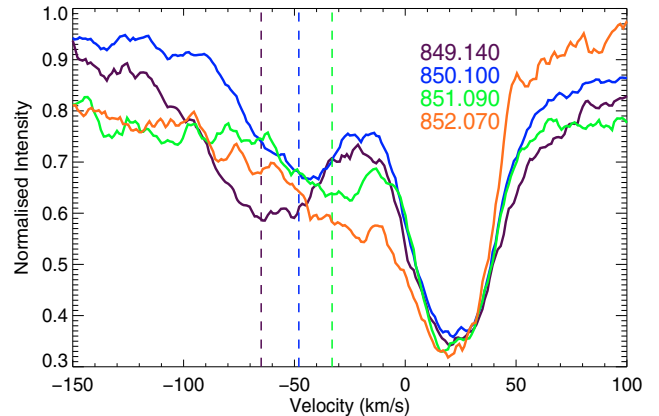


**Fig. 10.** Selected  $H\alpha$  emission line profiles on 17 to 20 January 2009 in the rest frame velocity of V351 Ori are overplotted. MHJD of the respective profiles are displayed using the same colours as of the profiles. Vertical dashed lines of different colours represent the centres of the BACs estimated by eye on the respective MHJDs. Red-shifted emission increased on MHJD 852.070 after the apparent disappearance of the outflow event.

red-shifted emission components, i.e. mostly type II and type III profiles (Fig. 5). The strength of both emission components varied during our observation, e.g. one of the component was always weaker compared to the other component and thus the shapes of the profiles also changed from one type to another. The average maximum velocities at the wings were  $\sim -250$   $\text{km s}^{-1}$  and  $\sim 250$   $\text{km s}^{-1}$  in the blue and red sides respectively. We also detected a strong outflow, which was clearly detectable from 17 to 19 January. The central narrow absorption component at  $\sim 20$   $\text{km s}^{-1}$  remained constant throughout the observations. We display the time evolution of the outflow in Fig. 10. The outflow gradually became wider as it continuously moved towards the central absorption. It is also worth to mention that the width of the central absorption was at its minimum among our observed spectra. The non-detection of the outflow on 20 January at MHJD 852.070 was most probably caused by the superposition of its line of sight with the central absorption. As a result, the central absorption became wider and asymmetric, e.g. it became elongated toward blue side and the red-shifted emission reached its maximum strength compared to the other spectra observed during 17 to 19 January, 2009.

### 3.8. Profile variations in March and April, 2009

Most of the profiles we observed on several days in March and April were double-peaked profiles (Fig. 6a). On 2 and 3 March 2009, there was a change in the slope of the blue-shifted emission. The red-shifted emission gradually gained strength and the profile evolved from type III-R to type II-R. The average maximum velocity at the blue wing was  $\sim -250$   $\text{km s}^{-1}$  and  $\sim 300$   $\text{km s}^{-1}$  at the red wing. We did not find any red-shifted emission on 29 March 2009 (MHJD 920.160). The profile showed a blue-shifted emission and the central absorption component. On the next day, we observed a strong red-shifted emission comparable to the blue one, and thus the profile was changed into a type II-R. The red-shifted emission was again considerably reduced on 31 March and we observed a type III-R profile. We detected a blue-shifted absorption component at  $\sim 71$   $\text{km s}^{-1}$  on 26 April 2009. The absorption component shifted towards the deep minima on 27 April. There was no signature of

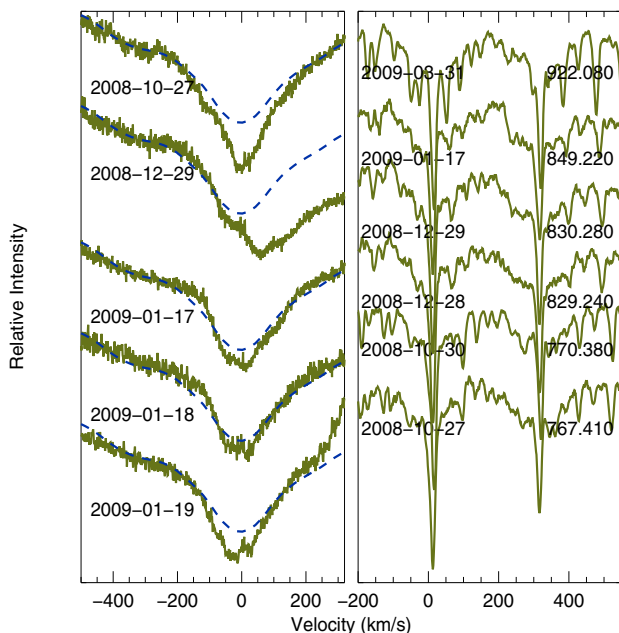


**Fig. 11.** a) Nightly average  $H\beta$  profiles of V351 Ori on several days. b) Sample NaD1 and NaD2 profiles of V351 Ori on a few epochs. Velocities are in the rest frame of V351 Ori.

outflow in the spectra on 28 April. The red-shifted emission became gradually stronger from 26 to 28 April and became comparable to the blue-shifted emission. These changes are similar to those observed on 28 and 29 December 2008 (Fig. 4), but the central absorption features were different, e.g. in April 2009 the central absorption component was broad and asymmetric and extended towards the red region compared to the narrow and nearly symmetric central absorption in December 2008.

### 3.9. Line profiles of $H\beta$ , NaD1, and NaD2

We obtained simultaneous spectra containing the  $H\beta$ , NaD1, and NaD2 profiles along with  $H\alpha$  emission line profiles. Due to the poor signal-to-noise ratio, we could not analyse the individual  $H\beta$  profiles. Instead, we plot the nightly average profiles of  $H\beta$  in the rest frame velocity of V351 Ori and overplot the synthetic spectra in Fig. 11a. The shape of the  $H\beta$  profiles also showed variations over the timescales of month. We did not find any emission components in the  $H\beta$  profiles within the noise level of our observed spectra. However, the prominent infall event occurred during 28 and 29 December, can be easily seen also in the  $H\beta$  line profiles. The NaD1 and NaD2 profiles displayed in Fig. 11b consist of a broad and a narrow absorption component. We did not find any elongated absorption in the broad line profiles. We measured the velocity of the narrow component and found that it was showing an almost constant velocity of  $\sim +22 \text{ km s}^{-1}$ , i.e. red-shifted by  $\sim 11 \text{ km s}^{-1}$ , compared to the star.

## 4. Discussion

Herbig Ae/Be stars show photometric variabilities on timescales of days to years. van den Ancker et al. (1996) analysed the long-term optical photometric behaviour of V351 Ori and found

that the star showed a large variation of  $>2$  mag before 1985. van den Ancker et al. also reported that the visual magnitude of V351 Ori varied by 0.16 mag between 1985 to 1990, i.e. over timescale of years. During 1990 to 1995, the visual magnitude of the star became almost constant without any significant variation. Balona et al. (2002) obtained the optical magnitudes (e.g.  $V \sim 8.92$ ,  $B - V \sim 0.37$ ,  $V - R \sim 0.22$  and  $V - I \sim 0.46$  mag) over timescales of minutes to weeks and did not find any significant variation within 0.05 mag. We obtained optical  $BVR/I$  photometry of the star on 11 November, 2009 and obtained the magnitudes  $V \sim 8.89$ ,  $B - V \sim 0.38$ ,  $V - R \sim 0.19$ , and  $V - I \sim 0.41$  mag, which indicates that there are no significant changes in the long-term photometric behaviour of V351 Ori. However, it is also noteworthy that our photometric observation did not coincide with the spectroscopic observation. Unlike the variations in visual magnitudes, which reflect the variable stellar photosphere, near infrared variability can account for changes in both the stellar photosphere and the circumstellar environments. Balona et al. (2002) compared the near infrared magnitudes of V351 Ori and found that  $H - K$  excess of V351 Ori (which serves as a proxy for the inner disk materials) decreased continuously over the period from 1982 to 2002. van den Ancker et al. (1996) and Balona et al. (2002) suggested that the systematic near infrared variability of V351 Ori is caused by the clearing of dust around the star, which indicates a variable circumstellar environment around V351 Ori.

Our high-resolution spectroscopic observations revealed the variable circumstellar environment and presences of TACs in the weak  $H\alpha$  emission line of the Herbig Ae star V351 Ori. As mentioned earlier, TACs in higher Balmer lines and in a few metallic lines have been detected in Herbig Ae stars such as BF Orionis, SV Cephei, WW Vulpeculae, XY Persei, and UX Orionis (Mora et al. 2002, 2004). All these Herbig Ae stars show prominent  $H\alpha$  emission profiles with equivalent widths ranging from  $-2.3 \text{ \AA}$  (for UX Ori) to  $-30.0 \text{ \AA}$  (for WW Vul) (Manoj et al. 2006). These stars also show optical photometric and polarimetric variabilities over timescales of months (Oudmaijer et al. 2001). XY Per, UX Ori, BF Ori, and WW Vul also show NIR variability over timescales of months (Eiroa et al. 2001). The characteristics of V351 Ori do not match the trend of the Herbig Ae stars mentioned above, because V351 Ori shows nearly constant optical magnitudes over years and a low  $H\alpha$  emission equivalent width ( $\leq 1 \text{ \AA}$ ). Moreover, V351 Ori is also comparatively older ( $\sim 6.5$  Myr) than the mentioned group of Herbig Ae stars with ages ranging from 2.5 to 5.2 Myr (Manoj et al. 2006; Montesinos et al. 2009). These differences make V351 Ori an interesting target to study the interaction of intermediate PMS stars (contracting towards the main sequence) with their circumstellar environment.

V351 Ori is known as an isolated Herbig Ae/Be star without any associated nebulosity in its immediate vicinity. However, (Hernández et al. 2005) suggested its association with the Ori OB1bc region located at a distance of 400 to 450 pc. The estimated ages of V351 Ori available in the literature vary from 1 to 6.5 Myr (van den Ancker et al. 1996; Ripepi et al. 2003). The main sources of uncertainty to estimate the age from the HR diagram is the distance to the star. The lower limit of the distance is  $\sim 210$  pc (van Leeuwen 2007) and the upper limit is  $\sim 450$  pc, which comes from the assumption of its association with the Ori OB1bc region (Hernández et al. 2005). Ripepi et al. (2003) analysed the pulsating behaviour of V351 Ori and suggested an intermediate value for the distance between the upper and lower limit, which leads to an estimate of the age of  $\sim 6.5$  Myr. The

**Table 2.** Transient absorption components appeared in the H $\alpha$  line profiles of V351 Ori.

Date yy-mm-dd	HJD (-2 454 000)	Cent. km s <sup>-1</sup>	Depth	Cent. km s <sup>-1</sup>	Depth
2008-10-27	767.32	-117.36	0.76	...	...
2008-10-27	767.36	-117.83	0.81	...	...
2008-10-27	767.41	-107.07	0.84	...	...
2008-12-29	830.10	157.50	0.34	-72.90	0.78
2008-12-29	830.13	150.07	0.34	-72.43	0.77
2008-12-29	830.17	148.40	0.33	-72.92	0.75
2008-12-29	830.21	139.74	0.37	-73.03	0.78
2008-12-29	830.25	140.74	0.38	-65.49	0.78
2008-12-29	830.28	138.41	0.39	...	...
2008-12-29	830.33	138.94	0.42	...	...
2009-01-17	849.11	-59.20	0.60	...	...
2009-01-17	849.14	-59.24	0.61	...	...
2009-01-17	849.18	-58.20	0.64	...	...
2009-01-17	849.22	-59.82	0.62	...	...
2009-01-18	850.10	-44.66	0.68	...	...
2009-01-18	850.13	-44.30	0.65	...	...
2009-01-18	850.29	-44.18	0.63	...	...
2009-01-18	850.32	-44.30	0.62	...	...
2009-01-19	851.09	-33.94	0.63	...	...
2009-01-19	851.13	-32.02	0.65	...	...
2009-01-19	851.23	-35.34	0.61	...	...
2009-01-19	851.27	-34.44	0.60	...	...
2009-01-19	851.35	-31.84	0.59	-103.79	0.73
2009-04-26	948.07	-55.88	0.61	...	...

H $\alpha$  emission from Herbig Ae/Bes, which is a proxy for active accretion, are found to decrease significantly beyond 3 Myr e.g. Manoj et al. (2006). There are some Herbig Ae/Be stars older than  $\sim 6$  Myr with significant H $\alpha$  emission (Manoj et al. 2006; Montesinos et al. 2009). However, the proposed age of V351 Ori i.e. 6.5 Myr seems to be consistent with the common trend of weak H $\alpha$  emission from stars with ages  $> 3$  Myr. We also consider that the mass of V351 Ori is  $2 M_{\odot}$  as estimated by Ripepi et al. (2003).

#### 4.1. Kinematics of transient absorption components (TACs)

Blue-shifted absorption components (BACs) and red-shifted absorption components (RACs) detected in H $\alpha$  emission line profiles of V351 Ori showed variation in the velocity centres, depths and widths of the profiles. We show the evolution of a RAC and BAC in Figs. 9 and 10 respectively. We tried to reproduce the observed H $\alpha$  profiles by fitting a multiple number of Gaussian components but we also noticed that the fitted Gaussians were not unique. When we tried to fit some profiles, e.g. the observed profiles of 29 to 31 March, 2009, we found that we got a good fit when we fitted two separate Gaussians to the blue-shifted and red-shifted emission components rather than a single Gaussian for the whole emission component. The fitting of these complicated and variable profiles for all observed spectra in a consistent way demands a complete understanding of the geometry of line-forming regions and their distribution with respect to the central star, which is beyond the scope of this work. Accordingly we measured the velocity centres and depths of the TACs' profiles by fitting Gaussian profiles to the individual TACs of the normalised spectra over the baseline of unity (obtained by the normalisation of the observed spectra by synthetic photospheric spectra). In this way, we estimated the velocity centres and depths of the individual component confidently, however, we could not estimate the FWHM of the individual

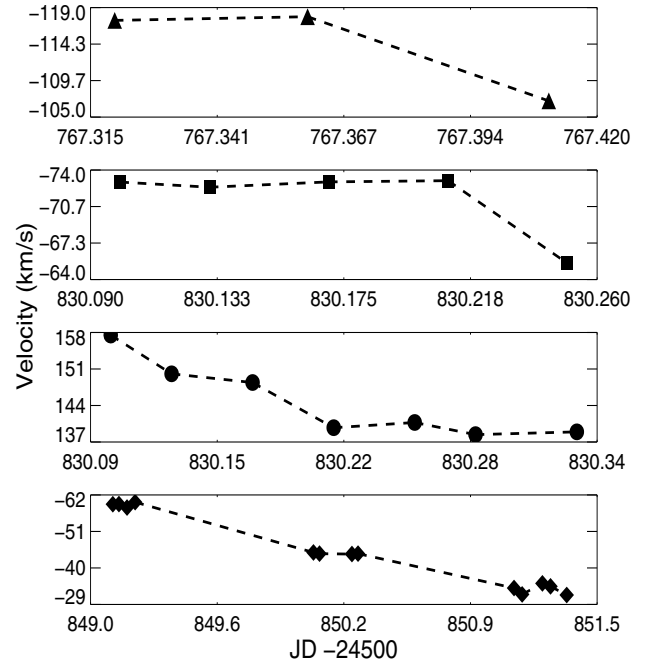


**Fig. 12.** Time evolution of the transient absorption components as they appeared in the H $\alpha$  line profiles. Triangles represent the outflow event on 27 October 2008, squares and circles represent the outflow and infall events respectively on 29 December 2008, and diamonds represent the outflow event during 17 to 19 January 2009.

TACs, which requires the fitting of the entire profile. As a result we discuss the kinematics of the observed TACs and not the physical conditions of the infalling and outgoing materials, because that partly depends on the values of the FWHM as well. It is also worth to mention that the detection and analysis of TACs in other Balmer lines such as H $\beta$ , H $\gamma$  etc. provides additional information. Because of the poor signal-to-noise ratio at H $\beta$  we could not detect the TACs as observed in the H $\alpha$  profiles. However, good temporal coverage of the spectroscopic observations helped to make an unambiguous detection of the TACs in the H $\alpha$  line profiles, and thus the kinematics of the TACs estimated from H $\alpha$  profiles only are also highly reliable. We list the velocity centres and depths of the transient absorption components from the normalised continuum level in Table 2. We plot the time evolution of the velocities of transient absorption components in Fig. 12. All detected transient absorption components in the H $\alpha$  line profiles showed deceleration of the gas at various rates. The rate of deceleration of the outflow event on 27 October 2008 was  $\sim 2 \text{ m s}^{-2}$ , for the infall event on 29 December 2008 it was  $\sim 1.7 \text{ m s}^{-2}$ , for outflow event it was  $\sim 2.2 \text{ m s}^{-2}$ , and for the outflow event during the 17 to 19 January 2009 it was fraction of  $\text{m s}^{-2}$ . Neither the magnetospheric accretion model nor the wind model provide any detailed explanation about the deceleration of the TACs. A detailed calculation of a time-dependent model considering accretion and wind models and including the observed results is very important to understand the variable star-disk interactions. Broad red-shifted absorption wings at high velocities are supposed to originate from the free fall of the surrounding material onto the star. The cool outflowing gas is supposed to originate farther away from the star than the accretion-dominated emission, but

still within about  $\sim 10 R_{\odot}$  (Edwards et al. 2003). We found that the average maximum velocity of the red-shifted emission wings was  $\sim 250$  to  $\sim 300 \text{ km s}^{-1}$ . We detected an enhanced red-shifted absorption wing extending up to  $\sim 380 \text{ km s}^{-1}$  on 29 December, 2009. Assuming the free-fall velocity condition, we estimate the extent of the region involved in the accretion processes as  $\sim 5 R_{\odot}$ , which indicates that the changes are taking place within a radius of  $\sim 0.02 \text{ AU}$ . Monnier & Millan-Gabet (2002) studied the dust sublimation radius of the pre-main sequence stars with a stellar radiation field. They discussed the relation between the size of the inner dusty disks and the luminosity of the central stars in the context of different disk models including the paradigm of both optically thick and thin inner disks. Considering the uncertainties such as the distance and thus the luminosity, and the model for optically thin/thick disks, the typical dust sublimation radius of V351 Ori would be in the range of  $\sim 0.07$  to  $.2 \text{ AU}$ . A comparison between the region of the gas accretion and the dust sublimation radius hint towards the presence of gaseous material in the inner disk cavity of V351 Ori. Further investigation of the inner disk properties of PMS stars such as V351 Ori will be helpful to understand the disk-dissipation processes and the associated timescales.

#### 4.2. Dust mass estimates using IRAS fluxes

The detection of red-shifted absorption wings that extend beyond  $300 \text{ km s}^{-1}$  supports a scenario of the accretion of surrounding materials onto the star. However, as V351 Ori also shows weak  $H\alpha$  emission, so it will be interesting to investigate whether the left-over gas in the circumstellar environment of the star is sufficient to continue the accretion. We estimate the dust mass and thus the gas mass in the circumstellar disk of V351 Ori using the Infrared Astronomical Satellite fluxes.

Dust grains present in the circumstellar environment absorb and scatter varying fractions of the incident photons ( $\lambda \leq 1 \mu\text{m}$ ) and re-emit part of the absorbed energy in the infrared band. Far infrared emission properties of the dust grains can be used to derive estimates on the amount of dust of the disks of pre-main sequence stars, assuming the emission at these wavelengths is optically thin. As suggested by Hildebrand (1983), the disk dust mass  $M_d$  can be computed using the relation

$$M_d = \frac{4\pi}{3} \frac{a \rho_d}{Q_v(T_d, a)} \frac{d^2 F_\nu(T_d)}{\pi B_\nu(T_d)},$$

where  $a$ ,  $\rho_d$  and  $d$  are the grain radius, specific grain mass density, and distance to the source, respectively.  $F_\nu$ ,  $Q_v(T_d, a)$ , and  $B_\nu(T_d)$  are the observed flux density, grain emissivity and the Planck function of temperature  $T_d$  at frequency  $\nu$ . van den Ancker et al. (1996) analysed the spectral energy distribution of V351 Ori, and estimated that the dust temperature corresponds to the far infrared Infrared Astronomical Satellite fluxes as 80 K. The far infrared spectral energy distribution of V351 Ori, peaks between 25 and 60  $\mu\text{m}$  and drops gradually between 60 and 100  $\mu\text{m}$ , which suggests that most of the emission arises beyond 25  $\mu\text{m}$ . In that case the calculation of dust grain temperature using 60 and 100  $\mu\text{m}$  flux densities (Helou & Walker 1988) would be a better estimate. Using the following relation,  $T_d = 49 \left( \frac{S_{60}}{S_{100}} \right)^{0.4}$  (Young et al. 1989), we estimated the dust grain temperature as 53 K. We adopted  $\rho_d = 3 \text{ g cm}^{-3}$ ,  $a = 0.1 \mu\text{m}$  and  $\frac{4a\rho_d}{3Q_v} = 0.024$  and  $0.04 \text{ g cm}^{-2}$  at 60 and 100  $\mu\text{m}$  respectively (Hildebrand 1983). The estimated dust masses at 60 and 100  $\mu\text{m}$  are  $9.5 \times 10^{-5}$  and  $9.2 \times 10^{-5} M_{\odot}$

respectively at an adopted distance of 450 pc and  $2.07 \times 10^{-5}$ , and  $2.01 \times 10^{-5} M_{\odot}$  at 210 pc. Assuming a gas-to-dust ratio of 100, the estimated disk mass (dust+gas) would be in the range of 0.002 to 0.009  $M_{\odot}$ . The estimated values of the disk mass of V351 Ori are lower compared to the disk mass of actively accreting Herbig Ae type stars such as AB Aur ( $0.01 M_{\odot}$ ), HD 163296 ( $0.028 M_{\odot}$ ) derived from millimetre observations (Mannings & Sargent 1997). This is consistent with the relatively evolved circumstellar environment of V351 Ori.

#### 4.3. Accretion and wind models

The  $H\alpha$  emission line serves as one of the most empirical signatures of accretion of the circumstellar material onto the central pre-main sequence stars. Magnetospheric accretion models are quite successful in explaining the observed spectral characteristics such as broad asymmetric line profiles etc. of accreting classical T Tauri stars (CTTS) i.e. the lower mass counterparts of Herbig Ae/Be (Hartmann et al. 1994; Muzerolle et al. 1998, 2001). According to magnetospheric accretion models, the stellar magnetic field disrupts the circumstellar disk at several stellar radii and the accreting material falls onto the stellar surface along the magnetic field lines Koenigl (1991). The results of magnetospheric accretion models suggest that the hydrogen emission lines form in the infall zone, so that the blue-shifted asymmetric emission-line profiles arise due to partial obscuration of the flow by the inner part of the accretion disk and the red-shifted absorption profiles result from infalling material at near free-fall velocities onto the stellar surface (Muzerolle et al. 1998). Muzerolle et al. (2004) also demonstrated the magnetically channelled disk accretion in the Herbig Ae star UX Ori and partly reproduced the double-peak  $H\alpha$  profile of UX Ori. Several studies e.g. Alencar et al. (2005); Kurosawa et al. (2006) found that disk wind also play an important role in the formation of double-peak profiles in CTTS.

V351 Ori showed varieties of  $H\alpha$  line profiles throughout our observation. The shape of the profiles contains information about the geometrical orientation and physical processes involved in the interaction of the star with its circumstellar environment. The common trends in all spectra are the slightly red-shifted central absorption and the elongated blue-shifted emission components. The width of the central absorption changed within a day. Though the strength of the blue-shifted emission component varied with time, but there was no significant variation in the maximum velocity at the wings. On the contrary, the red-shifted component showed drastic variations in shape, strength, and velocity. The strength of the red-shifted emission, if present, was less than the blue-shifted emission, which can be attributed to the selective absorption of the red-shifted flux due to the asymmetric distribution of the star-disk system with respect to our line of sight.

Kurosawa et al. (2006) investigated the formation of  $H\alpha$  emission line profiles around CTTS combining the magnetospheric accretion and disk-wind models (hybrid model). Though the  $H\alpha$  emission line profiles are calculated with typical parameters of CTTS, but it has also been suggested that the model can be used for other pre-main sequence stars such as Herbig Ae/Be stars and for Brown dwarfs (BDs). In order to understand the relative importance of the accretion and wind on the formation of the line profile Kurosawa et al. calculated the  $H\alpha$  line profiles for three cases e.g. the magnetospheric accretion, the disk wind, and a combination of magnetospheric accretion and disk wind models. With the use of this hybrid model Kurosawa et al. were able to reproduce the variety of

the  $H\alpha$  emission line profiles reported by Reipurth et al. (1996). Kurosawa et al. also discussed about the degeneracy in the line profiles which mostly emerged from the disk wind and the hybrid model. For example, the double peak  $H\alpha$  emission line profiles can be reproduced using the disk-wind model only. It is somewhat difficult to distinguish the contribution of magnetospheric accretion and disk winds in the emission line profiles. Alencar et al. (2005) reported the line profile variability of CTTS RW Aur and found significant variations in the intensity of the blue- and red-shifted emission components similar to V351 Ori. Alencar et al. tried to reproduce the double-peaked  $H\alpha$  emission line profiles with the magnetospheric accretion model and the disk wind model. The  $H\alpha$ ,  $H\alpha$ , and NaD1 profiles calculated using the disk wind models provided a better fit to the observed spectra. These studies reveal the importance of disk wind in the emission line profiles of the pre-main sequence stars. While the magnetospheric accretion model produces double-peak profile under certain conditions such as accretion rates etc., the wind model produces double-peak profiles in usual conditions (e.g. Alencar et al. 2005; Kurosawa et al. 2006). So it is possible that the disk wind contributes significantly in the  $H\alpha$  emission of V351 Ori, which showed a double-peak profile most of the time during our observation. However, we did not detect [O I]  $\lambda 6300$  Å emission in our observed spectra, which according to several authors forms in the disk wind (Hartigan et al. 1995). However, Acke et al. (2005) proposed that [O I]  $\lambda 6300$  Å emission arises in the surface layers of the protoplanetary disks surrounding Herbig Ae/Be stars due to the photodissociation of OH molecules. The maximum equivalent width of the  $H\alpha$  emission in our observed spectra is  $<1$  Å, which is less than the typical minimum equivalent width of the  $H\alpha$  emission, of  $\sim 4$  Å of the observed samples of Herbig Ae/Be stars studied by Acke et al. (2005). Considering the discrepancy regarding a thermal or non-thermal origin of the [O I]  $\lambda 6300$  Å emission and the low  $H\alpha$  emission, the absence of the line may not contradict with the presence of a disk wind. However, considering the rapid variation in the  $H\alpha$  emission on timescale of a day, which can be attributed to the variation of wind acceleration rate (Kurosawa et al. 2006), we propose that the disk wind may be responsible for most of the  $H\alpha$  emission of V351 Ori. However, the degeneracy of accretion and disk-wind models cannot be explored completely with our observed spectra.

We try to interpret the behaviour of V351 Ori in the context of hybrid model, i.e. by considering the effect of magnetospheric accretion as well as the disk-wind. The central absorption that was present in most of the spectra seemed to arise because of the geometrical configuration of the star-disk system which is viewed nearly edge-on. The changes in the shapes of the central absorption component, for most of the epochs, seemed to arise from the superposition of infall or outflow events in the same line of sight. On 27 October 2008, the  $H\alpha$  emission line profile may have been powered by a disk wind with the simultaneous presence of infall and outflow. The infall was quite prominent and it obscured the red-shifted emission component. Before 30 October 2008, the infall event ended and the central absorption returned to the normal shape with a nearly symmetric double-peak profile. On 28 and 29 December 2008, the  $H\alpha$  emission line profiles were dominated by the infall event. During 17 to 20 January 2009, the  $H\alpha$  emission line profiles were dominated by the disk wind but the blue-shifted emission was partially obscured by the prominent outflow event. The  $H\alpha$  emission line profiles observed during March and April 2009 also probably dominated by the disk wind. The  $H\alpha$  emission from

V351 Ori seems to originate in disk wind and at the same time sporadic infall of matter moderated by a magnetic field, and the outflow of cool gas occurs quite frequently.

## 5. Conclusion

Spectral analysis of 45 high-resolution spectra reveals that the line profile variability of V351 Ori is ubiquitous. The line profile variations are caused by changes in disk wind, wind acceleration, rate of accretion, and outflow of cool gaseous material. These signatures support the complex and dynamical interaction of the circumstellar material with V351 Ori. The circumstellar environment of the Herbig Ae star V351 Ori most probably consists of an inner cavity with gaseous material, a dusty disk and disk wind. The interaction processes are highly time-dependent from one hour for the changes in transient absorption components to one day and longer timescales of the order of months for the changes in the overall characteristics of the broad  $H\alpha$  profiles. Owing to the extensive time coverage of the observation down to timescales of hours we could follow the time evolution of the individual transient absorption components unambiguously. The long term monitoring of the star at timescales of months confirmed the deviation of the  $H\alpha$  emission line profiles from inverse P Cygni types. Accretion and outflow events are not continuous in nature, and the profiles of the TACs seem to be created by obscuration due to gaseous blobs, which indicate that the circumstellar environment of V351 Ori is inhomogeneous and clumpy in nature. Detectable changes in the transient absorption components showed a deceleration of the order of a fraction to a few  $\text{m s}^{-2}$ . Variation in the blue- and red-shifted emission components also occurred frequently on the shortest timescale of hours, which suggests the rate of the wind acceleration is also time-dependent. Finally, the presence of emission in the absence of veiling emphasises the importance of the disk wind in V351 Ori. Models containing dynamic and non-axisymmetric magnetospheric accretion with the disk wind may be able to provide a satisfactory explanation of the complex circumstellar activities of pre-main sequence stars.

*Acknowledgements.* The authors thank the anonymous referee for her/his insightful comments which helped to improve the presentation of the paper. This research has made use of the SIMBAD data base, operated at CDS, Strasbourg, France.

## References

- Acke, B., van den Ancker, M. E., & Dullemond, C. P. 2005, *A&A*, 436, 209
- Alencar, S. H. P., Basri, G., Hartmann, L., & Calvet, N. 2005, *A&A*, 440, 595
- Balona, L. A., Koen, C., & van Wyk, F. 2002, *MNRAS*, 333, 923
- de Winter, D., Grady, C. A., van den Ancker, M. E., Pérez, M. R., & Eiroa, C. 1999, *A&A*, 343, 137
- Dunkin, S. K., Barlow, M. J., & Ryan, S. G. 1997, *MNRAS*, 286, 604
- Edwards, S., Fischer, W., Kwan, J., Hillenbrand, L., & Dupree, A. K. 2003, *ApJ*, 599, L41
- Eiroa, C., Garzón, F., Alberdi, A., et al. 2001, *A&A*, 365, 110
- Helou, G., & Walker, D. W. 1988, *Infrared astronomical satellite (IRAS) catalogs and atlases, The small scale structure catalog*, 7
- Grady, C. A., Pérez, M. R., Talavera, A., et al. 1996, *A&AS*, 120, 157
- Grinin, V. P., The, P. S., de Winter, D., et al. 1994, *A&A*, 292, 165
- Grinin, V. P., Kozlova, O. V., Natta, A., et al. 2001, *A&A*, 379, 482
- Guimarães, M. M., Alencar, S. H. P., Corradi, W. J. B., & Vieira, S. L. A. 2006, *A&A*, 457, 581
- Hamann, F. 1994, *ApJS*, 93, 485
- Hamann, F., & Persson, S. E. 1992, *ApJS*, 82, 285
- Hartigan, P., Edwards, S., & Ghandour, L. 1995, *ApJ*, 452, 736
- Hartmann, L., Hewett, R., & Calvet, N. 1994, *ApJ*, 426, 669
- Hernández, J., Calvet, N., Hartmann, L., et al. 2005, *AJ*, 129, 856
- Hernández, J., Calvet, N., Hartmann, L., et al. 2009, *ApJ*, 707, 705

- Hildebrand, R. H. 1983, QJRAS, 24, 267
- Hubeny, I., & Lanz, T. 2000, Synspec User's Guides, Version 43,  
<http://nova.astro.umd.edu/Tlusty2002/pdf/syn43guide.pdf>
- Johns, C. M., & Basri, G. 1995, AJ, 109, 2800
- Koenigl, A. 1991, ApJ, 370, L39
- Kurosawa, R., Harries, T. J., & Symington, N. H. 2006, MNRAS, 370, 580
- Maheswar, G., Manoj, P., & Bhatt, H. C. 2002, A&A, 387, 1003
- Mannings, V., & Sargent, A. I. 1997, ApJ, 490, 792
- Manoj, P., Bhatt, H. C., Maheswar, G., & Muneer, S. 2006, ApJ, 653, 657
- Marconi, M., Ripepi, V., Alcalá, J. M., et al. 2000, A&A, 355, L35
- Monnier, J. D., & Millan-Gabet, R. 2002, ApJ, 579, 694
- Montesinos, B., Eiroa, C., Mora, A., & Merín, B. 2009, A&A, 495, 901
- Mora, A., Natta, A., Eiroa, C., et al. 2002, A&A, 393, 259
- Mora, A., Eiroa, C., Natta, A., et al. 2004, A&A, 419, 225
- Muzerolle, J., Calvet, N., & Hartmann, L. 1998, ApJ, 492, 743
- Muzerolle, J., Calvet, N., & Hartmann, L. 2001, ApJ, 550, 944
- Muzerolle, J., D'Alessio, P., Calvet, N., & Hartmann, L. 2004, ApJ, 617, 406
- Natta, A., Grinin, V. P., & Tambovtseva, L. V. 2000, ApJ, 542, 421
- Oudmaijer, R. D., Palacios, J., Eiroa, C., et al. 2001, A&A, 379, 564
- Rao, N. K., Sriram, S., Jayakumar, K., & Gabriel, F. 2005, JApA, 26, 331
- Reipurth, B., Pedrosa, A., & Lago, M. T. V. T. 1996, A&AS, 120, 229
- Ripepi, V., Marconi, M., Bernabei, S., et al. 2003, A&A, 408, 1047
- van den Ancker, M. E., The, P. S., & de Winter, D. 1996, A&A, 309, 809
- van Leeuwen, F. 2007, A&A, 474, 653
- Vieira, S. L. A., Corradi, W. J. B., Alencar, S. H. P., et al. 2003, AJ, 126, 2971
- Young, J. S., Xie, S., Kenney, J. D. P., & Rice, W. L. 1989, ApJS, 70, 699